JACC: BASIC TO TRANSLATIONAL SCIENCE VOL. 8, NO. 9, 2023

LEADING EDGE TRANSLATIONAL RESEARCH

PCSK9 Promotes Hypoxia-Induced EC Pyroptosis by Regulating Smac Mitochondrion-Cytoplasm Translocation in Critical Limb Ischemia

Meixin Zhang, MM,[a,*] Yixi Chen, PhD,[a,*] Yumin Qiu, PhD,[b] Jiapan Sun, PhD,[c] Jiang He, PhD,[b] Zhefu Liu, MM,[b] Jian Shi, PhD,[a] Wenbin Wei, MD,[a] Guifu Wu, PhD,[a] Jianwen Liang, PhD[a]

VISUAL ABSTRACT

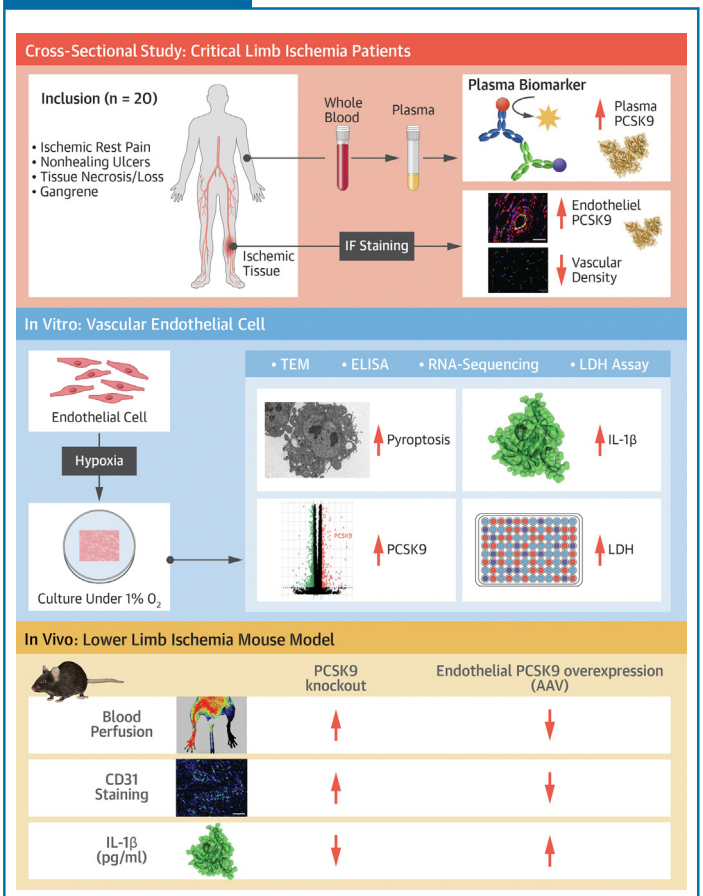

Zhang M, et al. J Am Coll Cardiol Basic Trans Science. 2023;8(9):1060–1077.

HIGHLIGHTS

- **Hypoxia-induced EC death and impaired angiogenesis are the main pathophysiological features of CLI. However, existing treatments have failed to significantly improve CLI. Therefore, it is necessary to deeply explore the mechanism underlying angiogenic dysfunction in ischemia.**
- **PCSK9 expression was significantly up-regulated in hypoxic ECs. The level of PCSK9 was elevated in patients with CLI. Suppressing the expression of PCSK9 attenuated hypoxia-induced pyroptosis and impaired angiogenesis. Mechanistically, PCSK9 aggravates hypoxia-induced vascular EC pyroptosis by regulating Smac mitochondrion-cytoplasm translocation in CLI.**
- **Additional studies will be required to clarify how PCSK9 mediates Smac mitochondria-cytoplasm translocation in HUVECs. In addition, whether the application of PCSK9 inhibitor could contribute to recovery in CLI also merits further clinical study and validation.**

From the [a]Department of Cardiology, The Eighth Affiliated Hospital, Sun Yat-sen University, Shenzhen, Guangdong, China; [b]Department of Hypertension and Vascular Disease, The First Affiliated Hospital, Sun Yat-sen University, Guangzhou, Guangdong, China; and the [c]Department of Geriatrics, Peking University Shenzhen Hospital, Shenzhen Peking University-The Hong Kong University of Science and Technology Medical Center, Shenzhen, Guangdong, China. *Drs Zhang and Chen have contributed equally to this work and are joint first authors.

ISSN 2452-302X https://doi.org/10.1016/j.jacbts.2023.05.016

SUMMARY

Hypoxia-induced endothelial cell death and impaired angiogenesis are the main pathophysiological features of critical limb ischemia. Mechanistically, proprotein convertase subtilisin/kexin type 9 (PCSK9) promoted Smac translocation from mitochondria to the cytoplasm. Inhibition of Smac release into the cytoplasm attenuated PCSK9-mediated hypoxia-induced pyroptosis. Functionally, PCSK9 overexpression impaired angiogenesis in vitro and reduced blood perfusion in mice with lower limb ischemia, but the effect was reversed by PCSK9 inhibition. This study demonstrates that PCSK9 aggravates pyroptosis by regulating Smac mitochondrion-cytoplasm translocation in the vascular endothelium, providing novel insights into PCSK9 as a potential therapeutic target in critical limb ischemia. (J Am Coll Cardiol Basic Trans Science 2023;8:1060–1077)

ABBREVIATIONS AND ACRONYMS

AAV = adeno-associated virus
CLI = critical limb ischemia
EC = endothelial cell
GSDM = gasdermin
LDL = low-density lipoprotein
mPTP = mitochondrial permeability transition pore
PAD = peripheral arterial disease
PCSK9 = Proprotein convertase subtilisin/kexin type 9
Smac = second mitochondria-derived activator of caspase

Critical limb ischemia (CLI), the most severe complication of peripheral artery disease, exerts a significant burden on health care resources.[1] Ischemia- and hypoxia-induced cell death and impaired angiogenesis are the main pathophysiological features of CLI.[2] Notably, vascular endothelial cells (ECs), which serve as the innermost layer of blood vessels and the most vulnerable cells to ischemia and hypoxia, play a pivotal role in the development of CLI.[3] Therefore, it is of great importance to explore the mechanism of ischemia- and hypoxia-induced EC injury in CLI.

Pyroptosis is a newly identified form of programmed cell death that differs from apoptosis and necroptosis.[4] The pyroptosis process is mediated by gasdermin (GSDM) family proteins and characterized by cell swelling and membrane perforation.[5] Endothelial pyroptosis is associated with the destruction of vascular endothelial integrity, inhibition of EC proliferation, and inhibition of angiogenesis.[6] However, whether ischemia and hypoxia in CLI have a profound effect on vascular EC pyroptosis remains to be elucidated.

Proprotein convertase subtilisin/kexin type 9 (PCSK9) is an essential molecule that regulates low-density lipoprotein (LDL) receptor recycling to maintain the balance of LDL cholesterol and has emerged as a risk predictor and a biotarget for atherosclerotic cardiovascular disease.[7,8] Recently, PCSK9 was identified as a downstream effector of hypoxia and found to be associated with endothelial dysfunction and vascular microthrombus formation.[9,10] Nevertheless, whether PCSK9 participates in vascular EC pyroptosis induced by hypoxia in CLI and the underlying mechanism have not been investigated.

Based on the uncertainties mentioned in the previous text, we hypothesized that PCSK9 promoted hypoxia-induced endothelial cell pyroptosis and resulted in impaired angiogenesis. To address this issue, PCSK9 levels in plasma and endothelium were examined in patients with CLI. PCSK9 expression under hypoxia was detected and the role of PCSK9 in hypoxia-induced pyroptosis was explored in vitro. Moreover, a lower limb ischemia mice model of PCSK9 knockout and adeno-associated virus (AAV)-mediated endothelial-specific PCSK9 overexpression was generated to investigate the effect of PCSK9 on angiogenesis in vivo. Mechanistically, we studied the potential function of PCSK9 on second mitochondria-derived activator of caspase (Smac) mitochondrion-cytoplasm translocation in regulating hypoxia-induced pyroptosis. This study may provide novel insights into the mechanism of CLI and demonstrate that PCSK9 might be a therapeutic target for the treatment of CLI.

METHODS

CELLS CULTURE. Human umbilical vein endothelial cells (HUVECs) were purchased from ICell Bioscience Inc and were maintained in endothelial cell medium (ECM) (ScienCell, 1001) supplemented with 10% fetal bovine serum under 5% CO_2 at 37 °C for routine culture. To induce hypoxia, cells were incubated in a controlled atmosphere chamber (UNITECH) with an atmosphere of 1% O_2/5% CO_2/94% N_2 at 37 °C. HUVECs at passages 3 to 8 were used for the

The authors attest they are in compliance with human studies committees and animal welfare regulations of the authors' institutions and Food and Drug Administration guidelines, including patient consent where appropriate. For more information, visit the Author Center.

Manuscript received February 24, 2023; revised manuscript received May 30, 2023, accepted May 31, 2023.

experiments in this study. The cell morphology was recorded by optical microscope.

TRANSMISSION ELECTRON MICROSCOPY. The membrane integrity of cells and mitochondria was observed by transmission electron microscopy (TEM). Images were collected on a HITACHI HT7700 transmission electron microscope equipped with a digital camera.

REAGENTS. Necrosulfonamide (NSA) (M9062), Z-VAD-FMK (M3143), Disulfiram (M3390) and Cyclosporine A (CsA, M1831) were purchased from AbMole. These reagents were dissolved in DMSO. The relative cell viability was normalized to those in the respective DMSO-treated wells.

CELL DEATH ANALYSIS. The cell death rate was detected with Annexin V-FITC/propidium iodide (PI) staining and flow cytometry (Cytoflex, Beckman Coulter). The cells were harvested by centrifugation (300 g/5 minutes) and washed with cold phosphate-buffered saline (PBS) (300 g/5 minutes) and 1× binding buffer (300 g/5 minutes) once each according to the manufacturer's instructions for an Apoptosis Detection Kit (BD Biosciences). After that, the cells were resuspended in 100 μL of 1× binding buffer and incubated with Annexin V-FITC (5 μL) and PI (5 μL) at room temperature in the dark for 15 minutes. The cells were added to 500 μL × binding buffer and tested by flow cytometry. The positive cell ratios were calculated and analyzed by FlowJo software (Tree Star Inc).

CELL VIABILITY ASSAY. The viability of HUVECs after hypoxia exposure was determined by the Cell Counting Kit-8 assay (CCK-8; CK04) according to the manufacturer's instructions. Briefly, cells seeded onto 96-well culture plates were incubated with 10 μL of CCK8 solution for 4 h. The optical density (OD) at 450 nm was measured with a microplate reader (TECAN). The fold change in cell viability was equal to 100% × (Ae - Ab)/(Ac - Ab), where Ae = $OD_{450\ nm}$ of the experimental group, Ab = $OD_{450\ nm}$ of the blank control, and Ac = $OD_{450\ nm}$ of the control group.

HOECHST 33342/PI STAINING. Cells were incubated with a mixed solution of Hoechst 33342 and PI (BL116A, Biosharp) for 20 minutes at 4 °C after 48 hours of plasmid transfection and then washed with cold PBS. The cells were observed under a fluorescence microscope (Leica DMI8).

siRNA TRANSFECTION. PCSK9 in HUVECs was transiently silenced by transfection of targeted siRNA using Lipofectamine 3000 (Thermo Fisher) according to the manufacturer's instructions. The siRNA sequences used are as follows:

- PCSK9 siRNA sense CCUCAUAGGCCUGGAGUUUAUTT
- PCSK9 siRNA antisense AUAAACUCCAGGCCUAUGAGGTT
- NC siRNA sense UUCUCCGAACGUGUCACGUdTdT
- NC siRNA antisense ACGUGACACGUUCGGAGAAdTdT

LENTIVIRAL TRANSFECTION. To establish stable PCSK9-knockdown ($PCSK9^{KD}$) cells, GV493 lentivirus containing a $PCSK9^{KD}$ sequence was transfected into HUVECs. Lentiviral transfection (multiplicity of infection = 5) was performed according to the manufacturer's instructions. After infection, the cells were selected using 1 μg/ml puromycin.

The sequence of LV-PCSK9i is as follows: 5′-CCTCATAGGCCTGGAGTTTAT-3′.

The sequence of LV-NC is as follows: 5'-TTCTCCGAACGTGTCACGT-3'.

PLASMID TRANSFECTION. PCSK9 was overexpressed utilizing pCMV-hPCSK9-3Flag, and the pCMV-3Flag empty vector was used as a control. Lipofectamine 3000 (Thermo Fisher) was used for cell transfection according to the manufacturer's instructions. Plasmids were used at a concentration of 50 ng/mL.

RNA ISOLATION AND REAL-TIME QUANTITATIVE POLYMERASE CHAIN REACTION. Total RNA was extracted using an EZ-press RNA purification kit (EZBioscience) following the manufacturer's protocol. Reverse transcription was performed using a Color Reverse Transcription Kit (EZBioscience), followed by the addition of iQ SYBR Green Supermix and analysis with an iQ5 real-time PCR detection system (Bio-Rad). The PCSK9-specific primer sequences were as follows: forward, 5′-AGTTGCCCCATGTCGACTAC-3′ and reverse 5′-GTAATCCGCTCCAGGTTCCA-3′. The following primer sequences were used: caspase3 sequences: forward 5′-CAGCTCATACCTGTGGCTGTG-3′ and reverse, 5′-TTATTAACGAAAACCAGAGCGCC-3′; caspase1 sequences: forward 5′-GCCCACCACTGAAAGAGTGA-3′ and reverse, 5′-TCTTCACTTCCTGCCCACAG-3′; GSDME sequences: forward 5′-ACAGGCCTTGGACTTTCCTG-3′ and reverse, 5′-GGACCGTGGGGTTTGAGAG-3′; GSDMD sequences: forward 5′-CCCGGATAAGAAGCAGAGGAC-3′ and reverse, 5′-GTCAGGAAGTTGTGGAGGCAC-3′; Smac sequences: forward 5′-GGCAGGTGATCATAGGAGCC-3′ and reverse, 5′-AGCTTCTGCTGCCATCTCTG-3′; and β-actin sequences: forward 5′-GCAGAAGGAGATCACTGCCCT-3′ and reverse, 5′-GCTGATCCACATCTGCTGGAA-3′. The mRNA level of the β-actin gene in each sample was measured as an internal normalization standard.

WESTERN BLOTTING. Total protein was extracted from HUVECs and quantified in RIPA buffer (Beyotime Biotechnology) containing PMSF (Beyotime Biotechnology). Mitochondrial proteins were extracted with a Mitochondria Isolation Kit (MP-007, Invent Biotechnologies). Protein extracts were subjected to SDS–PAGE, and the separated proteins were transferred to polyvinylidene fluoride membranes (Roche). The following antibodies were used: rabbit anti-hif-1a (1:1,000; Cell Signaling Technology), mouse anti-Caspase3 (1:1,000; Proteintech), rabbit anti-GSDME-N (1:1,000; Abcam), rabbit anti-Caspase1 (1:1,000; Cell Signaling Technology), rabbit anti-GSDMD-N (1:1,000; Affinity), rabbit anti-PCSK9 (1:1,000; Cell Signaling Technology), rabbit anti-PCSK9 (1:1,000; Proteintech), mouse anti-MLKL (1:10,000; Proteintech), rabbit anti-MLKL (phospho S358) (1:1,000; Abcam), rabbit anti-BCL-2 (1:1,000; Abcam), rabbit anti-Bax (1:3,000; Abcam), rabbit anti-NLRP3 (1:1,000; Proteintech), rabbit anti-ASC (1:20,000; Proteintech), rabbit anti-Smac (1:2,000; Proteintech), mouse anti-β-actin (1:1,000; Cell Signaling Technology), and rabbit anti-VDAC1 (1:3,000; Proteintech). Proteins were visualized with HRP-conjugated anti-rabbit IgG (1:3,000; Cell Signaling Technology) or HRP-conjugated antimouse IgG (1:3,000; Cell Signaling Technology), followed by use of an ECL system (Thermo). Analysis of the bands was performed using ImageJ software. β-actin was used to normalize the total protein data, and VDAC1 was used to normalize the mitochondrial protein data.

RNA SEQUENCING. HUVECs were cultured under hypoxic or normoxic conditions, and total RNA was collected with TRIZOL (Invitrogen). RNA quality was assessed on an Agilent 2100 bioanalyzer (Agilent Technologies) and checked using RNase-free agarose gel electrophoresis. After total RNA extraction, the eukaryotic mRNA was enriched with oligo(dT) beads, while prokaryotic mRNA was enriched by removing rRNA with a Ribo-Zero Magnetic Kit (Epicentre). Then, the enriched mRNA was fragmented into short fragments using fragmentation buffer and reverse transcribed into cDNA with random primers. Second-strand cDNA was synthesized with DNA polymerase I, RNase H, dNTP, and buffer. Then, the cDNA fragments were purified with a QiaQuick PCR extraction kit (Qiagen), followed by end repair, poly(A) addition, and ligation to Illumina sequencing adapters. The ligation products were size-selected by agarose gel electrophoresis, PCR amplified, and sequenced using the Illumina HiSeq2500 platform by Gene Denovo Biotechnology Co. We determined the differentially expressed genes (DEGs) in the 2 groups and performed gene ontology analysis.

LACTATE DEHYDROGENASE RELEASE ASSAY. Lactate dehydrogenase (LDH) release into the cell supernatant was assessed with an LDH Assay Kit (Solarbio, BC0685) according to the manufacturer's instructions.

ENZYME-LINKED IMMUNOSORBENT ASSAY FOR INTERLEUKIN-1β AND PCSK9. Culture media were collected and centrifuged to remove any cell debris or suspended cells. Mouse and human blood were collected after intervention. The serum of mice and the plasma of human were obtained after centrifugation at 3,000 rpm for 10 minutes at 4 °C. The levels of interleukin (IL)-1β released into the cell medium and serum were measured with IL-1β enzyme-linked immunosorbent assay kit (RayBiotech). PCSK9 secretion was measured with human PCSK9 enzyme-linked immunosorbent assay kit (RayBiotech).

MITOCHONDRIAL MEMBRANE POTENTIAL DETECTION. The mitochondrial membrane potential ($\Delta\Psi m$) was detected with JC-1 staining solution (Beyotime, C2006). Briefly, cells were seeded onto confocal dishes, treated with scrambled plasmid or PCSK9-overexpression plasmid, and cultured under normoxic conditions. After 48 hours, the cells were incubated with JC-1 staining solution for 20 minutes at 37 °C in a 5% CO_2 incubator. Images were captured with a laser scanning confocal microscope (LSM 880, Zeiss).

MITOCHONDRIAL PERMEABILITY TRANSITION PORE ASSAY. A total of 1×10^4 cells were cultured in confocal dishes and washed with PBS 2 times before the experiments. Then, an appropriate volume of Calcein AM staining solution, fluorescence quenching working solution, or ionomycin (100 μL) was added, and the cells were incubated at 37 °C for 30 minutes in the dark. After incubation, the culture medium was replaced with fresh medium, and the cells were incubated at 37 °C for 30 minutes in the dark and washed with PBS 3 times, after which detection buffer was added. The cells were observed under an LSM-880 confocal laser scanning microscope at 488 nm (LSM 880, Zeiss).

IN VITRO MIGRATION FUNCTION OF HUVECs. HUVEC migration was tested with 2 different methods. For the Transwell assay (Corning), HUVECs were digested and resuspended in serum-free ECM, and 2×10^4 cells were then loaded into the upper chambers of Transwells. The lower chambers were filled with ECM. After incubation at 37 °C for 6 hours under hypoxia, the

FIGURE 1 Hypoxia Induces Human Umbilical Vein Endothelial Cells Pyroptosis

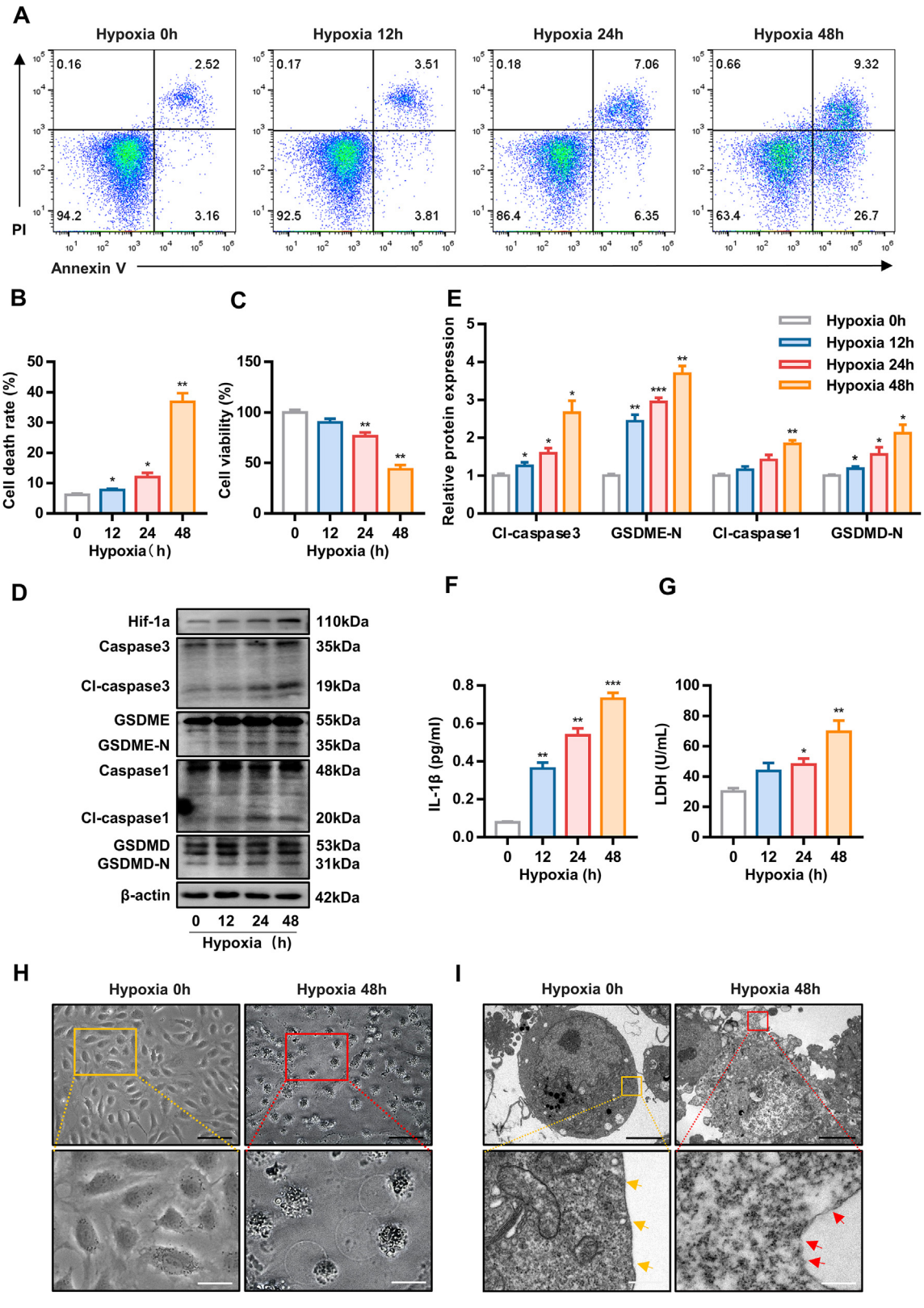

Continued on the next page

HUVECs were stained with crystal violet and counted in 5 random fields (magnification × 20) of each well. For the wound healing assay, 2×10^5 HUVECs were plated in a 6-well culture dish. A wound was created by manually scraping the cell monolayer with a p20 pipet tip, and the cell layer was washed once and supplemented with 1 mL of ECM. After 6 hours of incubation at 37 °C under hypoxia, the transmigrated cells were randomly observed under an optical microscope by independent investigators blinded to the treatment groups.

IN VITRO ADHESION FUNCTION OF HUVECs. A HUVEC adhesion assay was performed as described.[11] Dishes were coated with fibronectin (10 μg/mL). HUVECs (2×10^4) of the different groups were placed in each well of a 6-well plate and incubated for 6 hours at 37 °C under hypoxia. Nonattached cells were removed with PBS washing, and adherent HUVECs were fixed with 4% paraformaldehyde and stained with 0.3% crystal violet. The adherent HUVECs were randomly counted by independent investigators blinded to the treatment groups.

TUBE FORMATION ASSAY. For the tube formation assay, growth factor-reduced Matrigel (Corning) was warmed at 4 °C overnight. After the Matrigel had completely thawed, 60 μL of Matrigel was plated on 96-well plates to the same level for even distribution and incubated for 1 hour at 37 °C. HUVECs (3×10^4) were resuspended in ECM and loaded on top of the Matrigel. Each conditional group contained 3 wells. Following incubation at 37 °C for 6 hours under hypoxia, each well was imaged directly under a microscope, and the average number of tubules was determined from 3 to 5 random fields. Data were analyzed by ImageJ software.

IN VIVO ADENO-ASSOCIATED VIRUS–MEDIATED EC-SPECIFIC GENE OVEREXPRESSION. In vivo EC-specific gene overexpression was achieved with adeno-associated virus (AAV) vectors. Recombinant AAV vector carrying PCSK9 or empty vector with the TIE (pTIE) promoter (AAV-pTIE-PCSK9 or AAV-pTIE-empty) were manufactured by GeneChem. AAV-pTIE-empty served as a negative control. AAV-pTIE-PCSK9/empty vectors (5.0E+11 vector genomes/mice) were delivered via intravenous injection. Three weeks after AAV delivery, PCSK9 overexpression was verified by immunofluorescence staining and Western blotting.

MOUSE PRIMARY MOUSE AORTIC ENDOTHELIAL CELL CULTURE. Mouse primary mouse aortic endothelial cells were isolated from AAVENT-NC and AAVENT-PCSK9 mouse. For the initial culturing, Matrigel (Corning) was added to a 24-well plate and allowed to solidify at 37 °C for 20 minutes. The lumen side of aorta segments were placed down onto the collagen gel in ECM (ScienCell, 1001). The segments were removed on Day 4. After 3 to 4 days when outgrowth of cells was observed, the mouse primary mouse aortic endothelial cells were passaged using trypsin and reseeded on 0.1% gelatin-coated cell culture plates and cultured under 5% CO_2 at 37 °C.[12]

LOWER LIMB ISCHEMIA MODEL. C57BL/6J mice (wild-type), PCSK9-knockout ($PCSK9^{KO}$) mice, AAVENT-NC mice, and AAVENT-PCSK9 mice were used in this experiment. C57BL/6 mice were purchased from the Experimental Animal Center of Sun Yat-sen University. $PCSK9^{KO}$ mice were purchased from the Shanghai Model Organism Center. AAVENT-NC mice and AAVENT-PCSK9 mice on the C57BL/6J background were constructed with AAV injection. Mice at approximately 8 weeks of age were used in the experiment. The mice were housed under a 12-hour light/12-hour dark cycle. A lower limb ischemia model was generated as described in our previous study.[11,13] Briefly, the mice were anesthetized with 2.5% isoflurane, maintained with 1.5% isoflurane, and placed in dorsal recumbency with their hind limbs externally rotated. An incision was made in the skin over the femoral artery beginning at the inguinal ligament and continuing caudally to the popliteal bifurcation. The femoral artery was isolated above the level of the profunda and epigastric arterial branches,

FIGURE 1 Continued

(A to C) Cell death rate and cell viability of human umbilical vein endothelial cells under hypoxic conditions for 0, 12, 24, and 48 hours as determined by Annexin V/PI assay and CCK8 assay, respectively. **(D and E)** Effect of hypoxia on pyroptosis-related protein expression. **(F and G)** The concentration of interleukin (IL)-1β and lactate dehydrogenase (LDH) in the culture medium of human umbilical vein endothelial cells after 0, 12, 24, and 48 hours of hypoxia. **(H and I)** Representative morphological changes in human umbilical vein endothelial cells under normoxia or hypoxia for 48 hours, as captured by inverted microscopy (**black scale bar** = 100 μm, **white scale bar** = 10 μm) and transmission electron microscopy (**black scale bar** = 5 μm, **white scale bar** = 500 nm). Cells under normoxia show intact cell membranes **(yellow arrowheads).** Hypoxic cells show membrane disruption **(red arrowheads).** Data are expressed as mean ± SD. n = 3 per group, $^*P < 0.05$, $^{**}P < 0.01$, $^{***}P < 0.001$. Differences were compared to 0 hours. All data were analyzed using repeated measures analysis of variance with Dunnett's test.

FIGURE 2 PCSK9 is Up-Regulated in Human Umbilical Vein Endothelial Cells Under Hypoxia

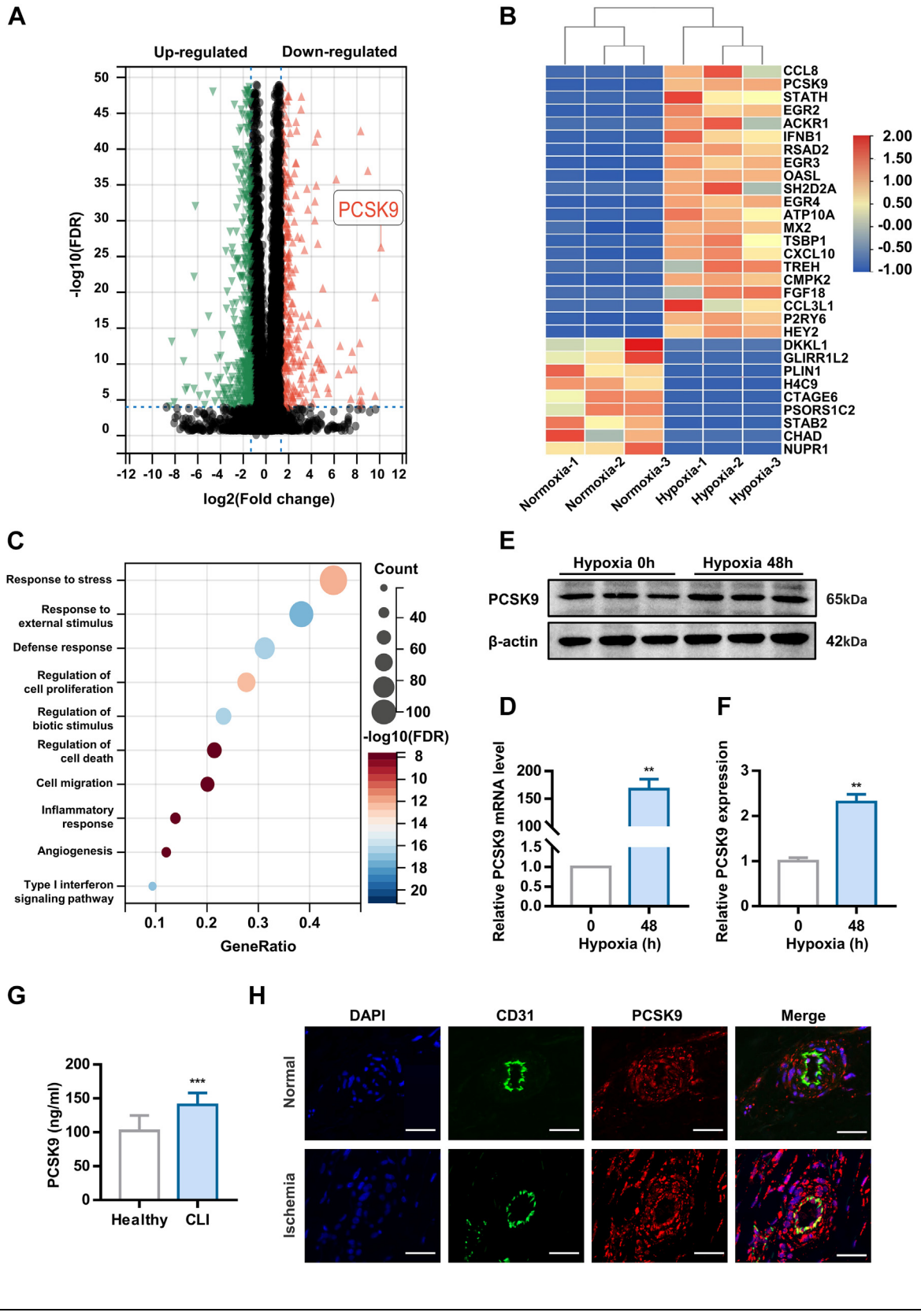

Continued on the next page

doubly ligated using 7-0 Prolene suture, and transected. The SFA caudal to the major branch points was dissected, ligated, and excised in its entirety. Lower limb subcutaneous blood flow was detected using a laser Doppler imager (Perimed Instruments) at 0, 3, 7, 14, and 21 days after surgery. After 21 days, the mice were sacrificed. The animal experiments were performed according to internationally followed ethical standards and had been approved by the Research Ethics Committee of The Eighth Affiliated Hospital, Sun Yat-sen University (2021d193).

HEMATOXYLIN AND EOSIN STAINING. The muscles were rapidly harvested, washed with normal saline, fixed in 4% formaldehyde, and then embedded in paraffin. The paraffin blocks were cut into 2-μm-thick sections and stained with hematoxylin and eosin. Images were acquired using an automatic digital slide scanning system (AxioScan.Z1, Zeiss) at 20× magnification.

IMMUNOFLUORESCENCE STAINING. Immunofluorescence staining was performed as described previously.[14] Briefly, cross sections (4-μm thick) of muscles and vessels were deparaffinized and rehydrated, and antigen retrieval was performed by microwave oven heating in 0.01 mol/L sodium citrate buffer (pH 6.0). All sections were incubated with CD31 antibody (Abcam, used at 1:50), α-SMA antibody (Proteintech, used at 1:200), PCSK9 antibody (HUABIO, used at 1:250) or isotype IgG antibody (Abcam, used at 2.5 μg/mL) overnight at 4 °C, followed by staining with Alexa Fluor 488-conjugated goat antirabbit secondary antibody (Invitrogen, Thermo Fisher, used at 4 μg/mL) or Alexa Fluor 594-conjugated goat antirabbit secondary antibody (Invitrogen, Thermo Fisher, used at 4 μg/mL). Nuclei were counterstained with DAPI. Immunofluorescence images were acquired using an automatic digital slide scanning system (AxioScan.Z1, Zeiss, Germany) at 20× magnification.

In addition, to detect the contribution of Smac in mitochondrion and cytoplasm, cells seeded onto confocal dishes were washed with ECM once. Then cells were incubated for 30 minutes at 37°C with 200 nmol/L Mito-Tracker Red CMXRos (Beyotime Biotechnology). After washing, cells were fixed for 15 minutes with 4% paraformaldehyde, permeabilized by 0.2% Triton X-100, and then incubated overnight at 4 °C with Smac antibodies in TBST containing 5% bovine serum albumin. After washing, the cells were incubated for 1 hour at room temperature with Alexa Fluor-labelled goat secondary antibodies at a dilution of 1:500. They were washed again, and then cells were observed under an LSM-880 confocal laser scanning microscope (LSM 880, Zeiss).

STUDY POPULATION. This study was approved by the Medical Ethics Committee of the Eighth Affiliated Hospital of Sun Yat-sen University (ZB-KYIRB-AF/SC-08/01.0). Patients were enrolled if they had been diagnosed with CLI. CLI status was determined based on the presence of ischemic rest pain in the foot or calf, nonhealing wound/ulcers, tissue necrosis or loss, or gangrene, along with evidence of hypoperfusion of the lower extremity, as identified by prior abnormal computed tomography angiography, magnetic resonance angiography, duplex ultrasound, resting toe systolic pressure (<50 mm Hg), ankle-brachial index (<0.9 or ≥1.3), or transcutaneous oxygen pressure (<30 mm Hg).[15] Patients with pregnancy, cancer, hepatic diseases, or HIV/AIDS were excluded. Healthy volunteers without known disease served as the controls.

HUMAN SAMPLES. Hindlimb muscles and vessels from patients who developed CLI were obtained from the Eighth Affiliated Hospital of Sun Yat-sen University. All tissues were collected according to policies of the Institutional Review Board under an approved protocol (ZB-KYIRB-AF/SC-08/01.0). The tissue sections were immunostained for PCSK9, CD31, and DAPI.

STATISTICAL ANALYSIS. Continuous variables were expressed as mean ± SD, whereas categorical variables were shown as n (%). The differences between categorical variables were evaluated with chi-square test. Shapiro-Wilk test was applied to analyze whether the continuous variables are normally

FIGURE 2 Continued

(A) Volcano plots of differentially expressed genes between the normoxia and hypoxia groups. **(B)** Heat-map analysis of the top 30 significant differentially expressed genes. **(C)** GO enrichment analysis of the top 250 differentially expressed genes. **(D to F)** PCSK9 mRNA and protein expression after 48 hours of hypoxia exposure. **(G)** The level of PCSK9 in plasma. **(H)** PCSK9 expression in vessels from critical limb ischemia patient as examined by immunofluorescence (scale bar = 50 nm). Data are expressed as mean ± SD. n = 3 per group in Data **D and F.** n = 20 per group in Data **G**. *P < 0.05, **P < 0.01, ***P < 0.001. In Data **D and F**, differences were compared to 0 hours. In Data **G**, differences were compared with Healthy. Data **D and F** were analyzed using paired Student's *t*-test. Data **G** were analyzed using Student's unpaired Student's *t*-test.

FIGURE 3 PCSK9 Is Involved in Hypoxia-Induced Pyroptosis

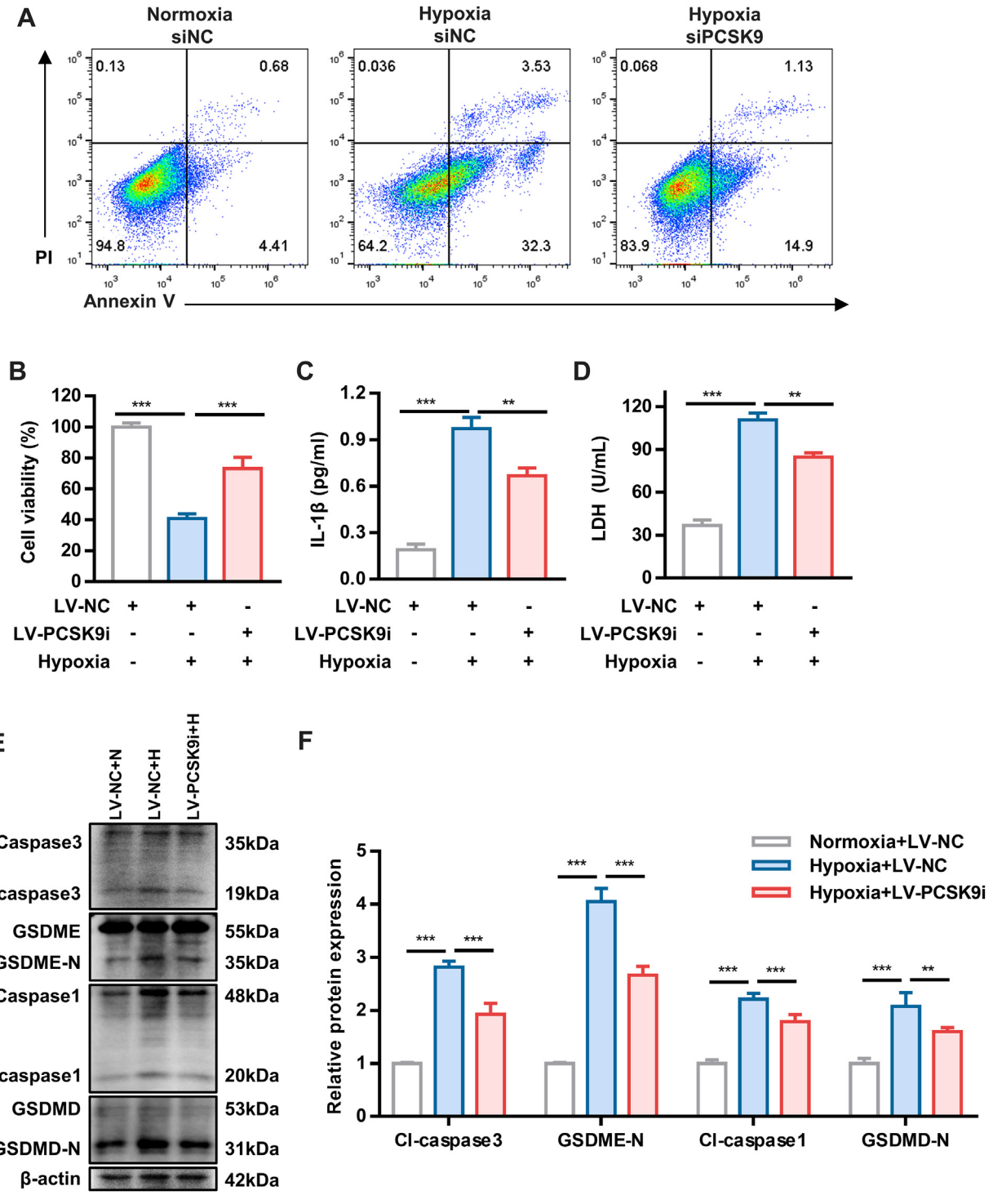

(A and B) Cell death rate and cell viability of PCSK9-knockdown ($PCSK9^{KD}$) human umbilical vein endothelial cells under hypoxia as detected by Annexin V/PI assay and CCK8 assay, respectively. **(C and D)** The concentration of interleukin (IL)-1β and lactate dehydrogenase (LDH) in $PCSK9^{KD}$ human umbilical vein endothelial cells under hypoxia. **(E and F)** Expression of pyroptosis-related proteins in $PCSK9^{KD}$ human umbilical vein endothelial cells under hypoxia. Data are expressed as mean ± SD. n = 3 per group, $^{*}P < 0.05$, $^{**}P < 0.01$, $^{***}P < 0.001$. Differences were compared with hypoxia LV-NC group. All data were analyzed using 1-way analysis of variance followed by Tukey's post hoc analysis.

distributed. Homogeneity of variance was evaluated before 1-way analysis of variance (ANOVA). Student's *t*-test was performed for evaluating differences between 2 groups, and paired Student's *t*-test was adopted for pair samples. One-way ANOVA followed by Tukey's post hoc test or Dunnett's test (if only comparing to the control group), or repeated measures ANOVA was used for multiple pairwise comparisons. A P value <0.05 was considered statistically significant. False discovery rate was further calculated using Benjamini-Hochberg methods. All statistical analyses were performed using GraphPad Prism software (GraphPad Prism version 8.0.1).

RESULTS

HYPOXIA INDUCES HUVEC PYROPTOSIS. To assess the effect of hypoxia on HUVECs, cells were exposed to hypoxia for 0, 12, 24, or 48 hours. A progressive, time-dependent increase in the cell death rate was detected by Annexin V/PI assay (**Figures 1A and 1B**). Similarly, cell viability decreased over time; specifically, cell viability declined rapidly at 48 hours (**Figure 1C**).

Apoptosis and necroptosis are well-known forms of cell death induced by hypoxia. Notably, pyroptosis, a recently identified form of programmed cell death, was recently reported to be involved in the effects of hypoxia.[16] Pyroptosis is characterized by the formation of pores in the plasma membrane that lead to the release of LDH and proinflammatory cytokines such as interleukin (IL)-1β.

To explore which forms of cell death predominate in hypoxia-induced cell death, we detected mediators of these forms. Immunoblot analysis of characteristic protein markers revealed that hypoxia increased the level of pyroptosis (cleaved caspase3, GSDME-N, cleaved caspase1, GSDMD-N) (**Figures 1D and 1E**, Supplemental Figures 1A to 1D). Moreover, we utilized CCK8 assay to examine the cell viability in the presence of a necroptosis inhibitor (NSA), an apoptosis inhibitor (Z-VAD-FMK), and a pyroptosis inhibitor (Disulfiram) under hypoxia. The optimal concentrations of NSA, Z-VAD-FMK, and Disulfiram were determined by CCK8 assay (Supplemental Figures 1E to 1G). The data showed that Disulfiram greatly decreased cell death (Supplemental Figures 1H to 1J).

Further studies revealed that the concentrations of IL-1β and LDH in the culture medium increased gradually during hypoxia (**Figures 1F and 1G**). Hypoxia led to cell swelling and membrane rupture (**Figures 1H and 1I**). These results indicate that hypoxia induces pyroptosis in vascular ECs.

PCSK9 MEDIATES HYPOXIA-INDUCED PYROPTOSIS. To investigate the potential regulatory genes involved in hypoxia-induced pyroptosis, RNA sequencing was carried out with cells subjected to normoxia or hypoxia for 48 hours. Significant DEGs, identified based on a fold change >2.5 and false discovery rate <0.0001, are shown in **Figure 2A**. The top 30 DEGs are presented in **Figure 2B** in the form of a heatmap. Gene ontology enrichment analysis revealed that the DEGs were mainly enriched in the response to stress, cell death, angiogenesis, and inflammation (**Figure 2C**). PCSK9 is a key regulator of LDL cholesterol metabolism.[17] However, a randomized controlled trial recently showed that inhibiting PCSK9 could reduce the risk of CLI.[18] Consequently, we explored whether PCSK9 participates in the process of EC pyroptosis induced by hypoxia. To validate the RNA sequencing results, the expression of PCSK9 was determined via real-time quantitative polymerase chain reaction (RT-qPCR) and Western blotting (**Figures 2D to 2F**). Additionally, we collected muscles from the ischemic hindlimb of CLI patient who underwent amputation. The characteristics of the volunteers are shown in Supplemental Table 1. The vessel density was significantly decreased in the distal hypoxic muscles (Supplemental Figure 2). Further studies showed that CLI patients had a higher plasma PCSK9 concentration than healthy control subjects (**Figure 2G**). The expression of PCSK9 was also higher in the distal hypoxic vascular endothelium than in the proximal normal vascular endothelium (**Figure 2H**). Therefore, the data in the previous text demonstrate that PCSK9 expression is elevated during hypoxia.

To further investigate whether PCKS9 is involved in hypoxia-induced pyroptosis, $PCSK9^{KD}$ HUVECs were generated by siRNA and lentivirus infection. The efficiency of PCSK9 knockdown was validated by RT-qPCR and Western blotting (Supplemental Figures 3A to 3D). Silencing of PCSK9 expression protected cells from hypoxia-induced cell death (**Figures 3A and 3B**, Supplemental Figure 4). The expression of pyroptosis-related proteins was partially reduced in hypoxic HUVECs transfected with LV-PCSK9i, but not necroptosis-related and apoptosis-related proteins (**Figures 3E and 3F**, Supplemental Figure 5). Additionally, knockdown of PCSK9 decreased the release of IL-1β and LDH into the culture medium (**Figures 3C and 3D**). These findings suggested that inhibition of PCSK9 ameliorated the inflammatory response and hypoxia-induced pyroptosis. Collectively, our findings indicate that PCSK9 may play an important role in hypoxia-induced pyroptosis.

FIGURE 4 **PCSK9 Overexpression Leads to Human Umbilical Vein Endothelial Cells Pyroptosis**

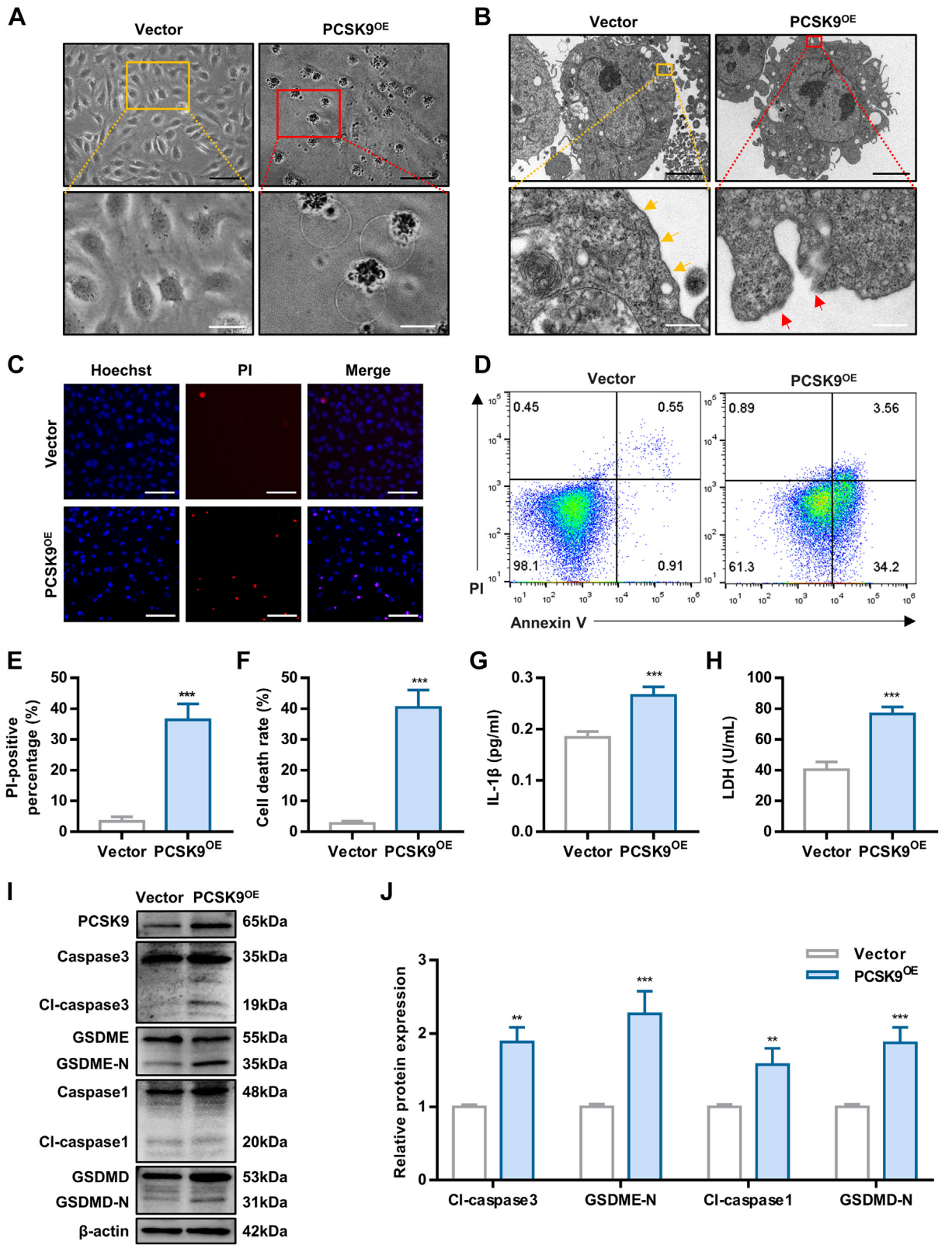

Continued on the next page

PCSK9 REGULATES HYPOXIA-INDUCED PYROPTOSIS BY MEDIATING SMAC MITOCHONDRION-CYTOPLASM TRANSLOCATION. Next, we investigated whether PCSK9 could induce pyroptosis under normoxia. HUVECs were transfected with the PCSK9-overexpression plasmid, and the transfection efficiency was confirmed by RT-qPCR and western blotting (Supplemental Figures 6A and 6B). Morphological analysis showed that PCSK9-overexpressing ($PCSK9^{OE}$) cells underwent pyroptosis, which was accompanied by cellular swelling and disruption of the cell membrane (**Figures 4A and 4B**). Overexpression of PCSK9 induced a dramatic increase in cell death, as evaluated by Hoechst/PI staining and an Annexin V/PI assay (**Figures 4C to 4F**). The increase in extracellular IL-1β and LDH release also indicated the occurrence of pyroptosis in the $PCSK9^{OE}$ cells (**Figures 4G and 4H**). To further verify the involvement of PCSK9 in pyroptosis, pyroptosis-related protein levels were detected by Western blotting. As shown in **Figures 4I and 4J**, the levels of pyroptosis-related proteins, including cleaved caspase3, GSDME-N, cleaved caspase1, and GSDMD-N, were up-regulated. In total, our results indicate that PCSK9 induces pyroptosis in HUVECs.

The mitochondrial pathway was recently reported to be important for pyroptosis.[19] Compared with that in the vector group, the mitochondrial ultrastructure was severely damaged in $PCSK9^{OE}$ cells, with mitochondrial swelling and disruption of membrane continuity (**Figure 5A**), indicating that PCSK9 may impact the mitochondria. Therefore, we hypothesized that PCSK9 mediates pyroptosis via the mitochondrial pathway. Then, mitochondrial function was detected. PCSK9 overexpression led to the opening of mitochondrial permeability transition pores (mPTPs) and a decrease in $\Delta\Psi m$ (**Figures 5B and 5D**). Treatment with CsA (10umol/L) a potent inhibitor of mitochondrial permeability transition, partially reversed the impairment of mitochondrial function (**Figures 5C and 5E**).[20] Thus, PCSK9 impairs mitochondrial morphology and function.

Then, we explored the specific mechanisms by which PCSK9 mediates hypoxia-induced pyroptosis. Smac functions by activating caspase and was recently reported to be involved in pyroptosis.[21,22] In response to cell death stimuli, Smac is released from mitochondria and moves to the cell plasma, which is followed by the opening of mPTPs. PCSK9 overexpression promoted Smac expression, whereas PCSK9 knockdown significantly suppressed it, as predicted (**Figures 5F and 5G**). We assumed that after its transfer to the cytoplasm, Smac interacted with caspases to mediate pyroptosis. As shown in **Figures 5H to 5K**, PCSK9 facilitated the translocation of Smac from the mitochondria to the cytosol, and this effect was reversed after the knockdown of PCSK9. Immunofluorescence staining showed similar results (**Figure 5L**). However, the translocation of Smac in $PCSK9^{OE}$ cells was inhibited by CsA (**Figure 5L**). Next, cells transfected with the $PCSK9^{OE}$ plasmid were cultured under hypoxia. Pyroptosis was attenuated in the cells treated with CsA, as shown by the decreasing release of IL-1β and LDH (**Figures 5M and 5N**). This result was further confirmed by an assessment of protein expression (**Figures 5O and 5P**). Because $PCSK9^{OE}$ cells showed higher levels of IL-β, PCSK9 may play a role through NLRP3 inflammasome. As shown in Supplemental Figure 7, the expression of NLPR3 and ASC were up-regulated in $PCSK9^{OE}$ cells.

Because the translocation of mitochondrial proteins was mainly related to BAX- and BAK- dependent mitochondrial permeability transition pore (mPTP) opening,[23,24] we hypothesized that PCSK9 may induce Smac translocation through triggering mPTP opening. Further study showed that PCSK9 increased the expression of BAK, which is essential in mPTP opening and might be involved in PCSK9-induced Smac translocation (Supplemental Figure 8). Taken together, these results indicate that PCSK9 regulates hypoxia-induced pyroptosis by mediating Smac translocation from the mitochondria to the cytoplasm.

INHIBITION OF PCSK9 INCREASES ANGIOGENESIS UNDER HYPOXIC CONDITIONS. Impaired angiogenesis induced by ischemia and hypoxia is the main pathophysiological feature of CLI. To investigate the influence of PCSK9 on angiogenesis, we detected

FIGURE 4 Continued

(A) Representative morphology of $PCSK9^{OE}$ human umbilical vein endothelial cells captured by inverted microscopy (**black scale bar** = 100 μm, **white scale bar** = 10 μm). **(B)** $PCSK9^{OE}$ human umbilical vein endothelial cells captured by TEM (scale bar = 5 μm, **white scale bar** = 500 nm). **Yellow arrowheads** indicate intact cell membranes, whereas **red arrowheads** indicate ruptured membranes. **(C and E)** Representative fluorescence microscopic images of cells stained with Hoechst/PI to evaluate the effect of PCSK9 overexpression on cell death (scale bar = 100 μm) and quantification of the percentage of PI-positive cells. **(D and F)** Cell death rate of $PCSK9^{OE}$ cells as detected by Annexin V/PI assay. **(G and H)** The concentration of interleukin (IL)-1β and lactate dehydrogenase (LDH) in the culture medium of $PCSK9^{OE}$ cells. **(I and J)** Effect of PCSK9 overexpression on pyroptosis, as detected by Western blotting. Data are expressed as mean ± SD. n = 3 per group, *P < 0.05, **P < 0.01, ***P < 0.001. Differences were compared to Vector. All data were analyzed using unpaired Student's t-test.

FIGURE 5 PCSK9 Regulates Hypoxia-Induced Pyroptosis by Mediating Smac Mitochondrion-Cytoplasm Translocation

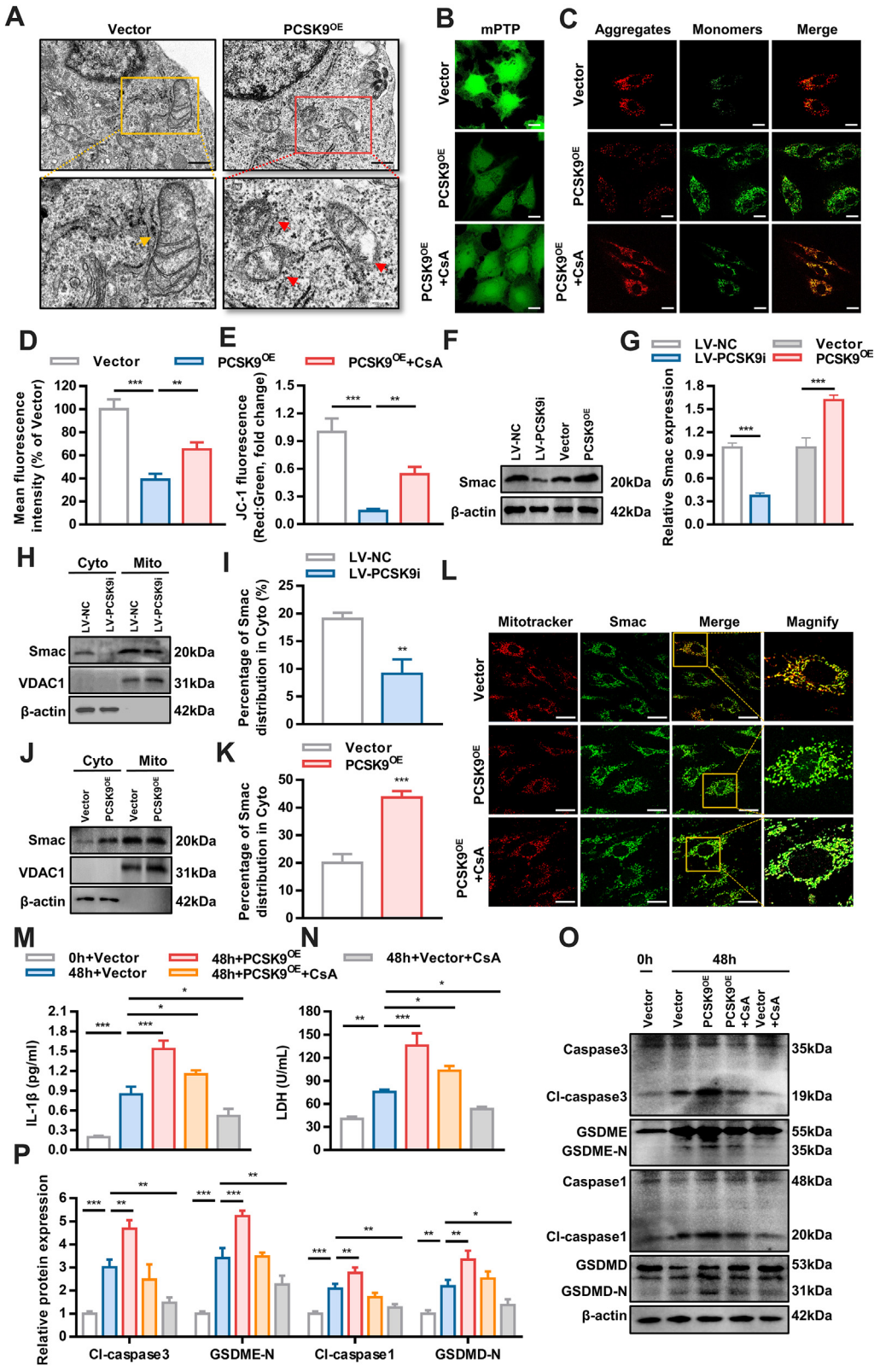

Continued on the next page

angiogenesis capacity in vitro. The migration, adhesion and tube formation capacities of vascular ECs were increased in the PCSK9^{KO} group but were inhibited in the AAVENT-PCSK9 group under hypoxia (**Figures 6A to 6H**). In addition, we established a lower limb ischemia model in vivo. The efficiency of PCSK9 overexpression induced by AAV injection into mice was verified by immunofluorescence staining and Western blotting (**Figures 7A and 7B**, Supplemental Figure 9). Blood perfusion and the vessel density were restored in the PCSK9^{KO} mice, whereas blood flow was significantly decreased in the AAVENT-PCSK9 mice, accompanied by increased muscle fiber necrosis (**Figures 7C to 7G**, Supplemental Figure 10). The limb salvage ratio was better in the PCSK9^{KO} groups, whereas limb loss and foot necrosis were much more prevalent in the AAVENT-PCSK9 groups (**Figure 7H**). Moreover, a substantial amount of IL-1β was detected in the AAVENT-PCSK9 mice, whereas the level of IL-1β in the PCSK9^{KO} mice was not significantly different from that in the wild-type mice, indicating that PCSK9 induced pyroptosis in mice with lower limb ischemia (**Figure 7I**). These findings suggest that PCSK9 was detrimental to ischemic hindlimb recovery.

DISCUSSION

The major findings of our in vitro and in vivo experiments are as follows: 1) hypoxia induces HUVEC pyroptosis; 2) PCSK9 mediates hypoxia-induced pyroptosis; 3) PCSK9 regulates hypoxia-induced pyroptosis by mediating Smac mitochondrion-cytoplasm translocation; and 4) inhibition of PCSK9 enhances angiogenesis in vivo and in mice with lower limb ischemia. Our study indicates that PCSK9 may be a novel therapeutic target for CLI.

In ischemia, angiogenesis capacity is impaired, which is closely related to an increase in the unnatural death of vascular ECs and influences the progression and prognosis of diseases and conditions, such as wound healing and gangrene.[25,26] Studies have shown that VEGF could promote angiogenesis and improve limb blood flow in an animal model of hindlimb ischemia.[27] However, VEGF has failed to significantly improve peripheral arterial disease (PAD) in randomized clinical trials, suggesting that the involvement of angiogenesis in lower limb ischemia and its relationship with VEGF have not been thoroughly studied.[28] Therefore, it is necessary to explore the mechanism underlying angiogenic dysfunction in ischemic in depth.

Hypoxia induces excessive cell death, thereby inhibiting angiogenesis. Evidence shows that apoptosis and necroptosis are classic mechanisms underlying this effect. Pyroptosis is an important type of cell death that is related to inflammation.[29] Many studies have demonstrated that pyroptosis affects cell proliferation and *in vitro* functions, such as migration and adhesion, whereas hypoxia can lead to pyroptosis.[30] Despite the fact that ECs directly perceive changes in blood oxygen, few studies have focused on the role of the vascular endothelium in hypoxia-induced pyroptosis. We found that hypoxia mainly induced the pyroptosis of ECs and impaired angiogenesis. However, the underlying mechanism remains unknown. Therefore, we investigated the mechanism by which hypoxia induces vascular EC pyroptosis.

PAD is associated with abnormal lipid metabolism, and CLI occurs with disease progression. PCSK9 inhibits LDL degradation by binding low-density lipoprotein receptor.[31] Injection of PCSK9 inhibitors reduces LDL levels in patients with hyperlipidemia. Recently, the multiple functions of PCSK9 have attracted increasing attention. A randomized controlled trial showed that the application of a PCSK9 inhibitor could reduce the risk of PAD, including CLI, by 30% and improve ischemic symptoms.[18] A previous study demonstrated that PCSK9 regulates the pyroptosis of smooth muscle cells in

FIGURE 5 Continued

(A) Transmission electron microscopy of mitochondria in PCSK9^{OE} cells (**black scale bar** = 500 μm, **white scale bar** = 250 μm). **Yellow arrowheads** indicate intact mitochondria, whereas **red arrowheads** indicate mitochondria with a ruptured membrane. **(B and D)** Changes in mitochondrial permeability transition pore opening. **(C and E)** Representative confocal microscopic images of PCSK9^{OE} cells stained with JC-1 to detect the mitochondrial membrane potential (MMP) and quantification of JC-1 fluorescence **(red-to-green ratio)** showing changes in fluorescence intensity with different treatments (scale bar = 20 μm). **(F and G)** Western blot analysis of Smac levels after PCSK9 knockdown or overexpression. **(H to K)** The effect of PCSK9 overexpression and knockdown on the distribution of Smac in the cytoplasm and mitochondria as determined by Western blotting. **(L)** The intracellular distribution of Smac as examined by immunofluorescence. **(M and N)** The concentration of IL-1β and LDH in the culture medium of PCSK9^{OE} cells treated with CsA. **(O and P)** Effect of CsA-medicated suppression of Smac translocation on PCSK9^{OE} cell pyroptosis, as detected by Western blotting. Data are expressed as mean ± SD. n = 3 per group, *P < 0.05, **P < 0.01, ***P < 0.001. In Data **D and E**, differences were compared to PCSK9^{OE}. In Data **G, I, and K**, differences were compared between LV-NC and LV-PCSK9i, or between Vector and PCSK9^{OE}. In Data **M, N, and P**, differences were compared with 48h+Vector. Data **G, I, and K** were analyzed using unpaired Student's *t*-test. Other data were analyzed using 1-way analysis of variance followed by Tukey's post hoc analysis.

FIGURE 6 PCSK9 Inhibition Increases Angiogenesis In Vitro

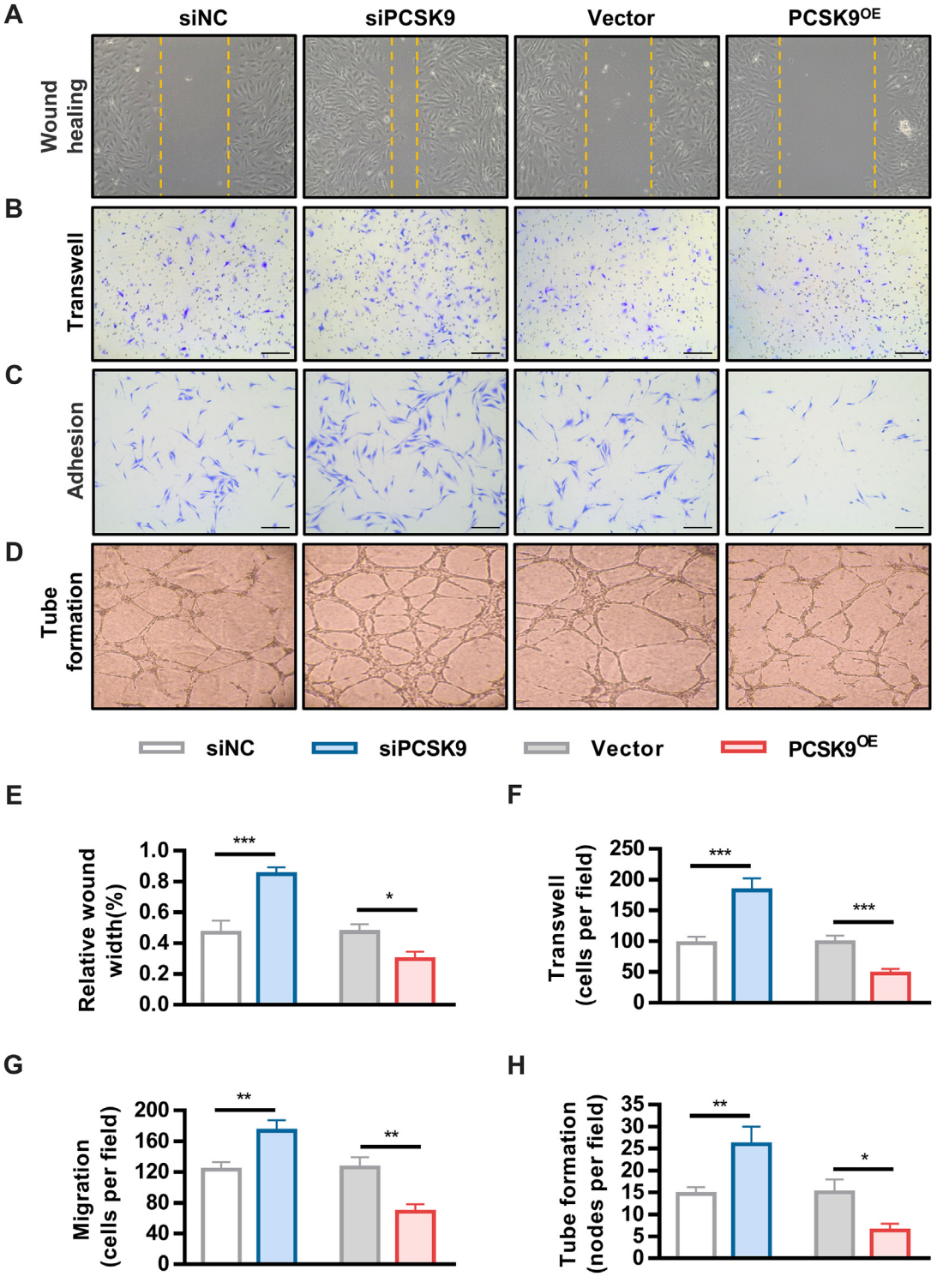

Representative images and quantification analysis of wound healing **(A and E)**, migration **(B and F)**, adhesion **(C and G)** and tube formation **(D and H)** in PCSK9^{KD} and PCSK9^{OE} cells. Data are expressed as mean ± SD. n = 3 per group, *$P < 0.05$, **$P < 0.01$, ***$P < 0.001$. Differences were compared siPCSK9 to siNC, or PCSK9^{OE} to Vector. All data were analyzed using Student's unpaired Student's *t*-test.

FIGURE 7 PCSK9 Inhibition Improves Blood Perfusion in a Mouse Lower Limb Ischemia Model

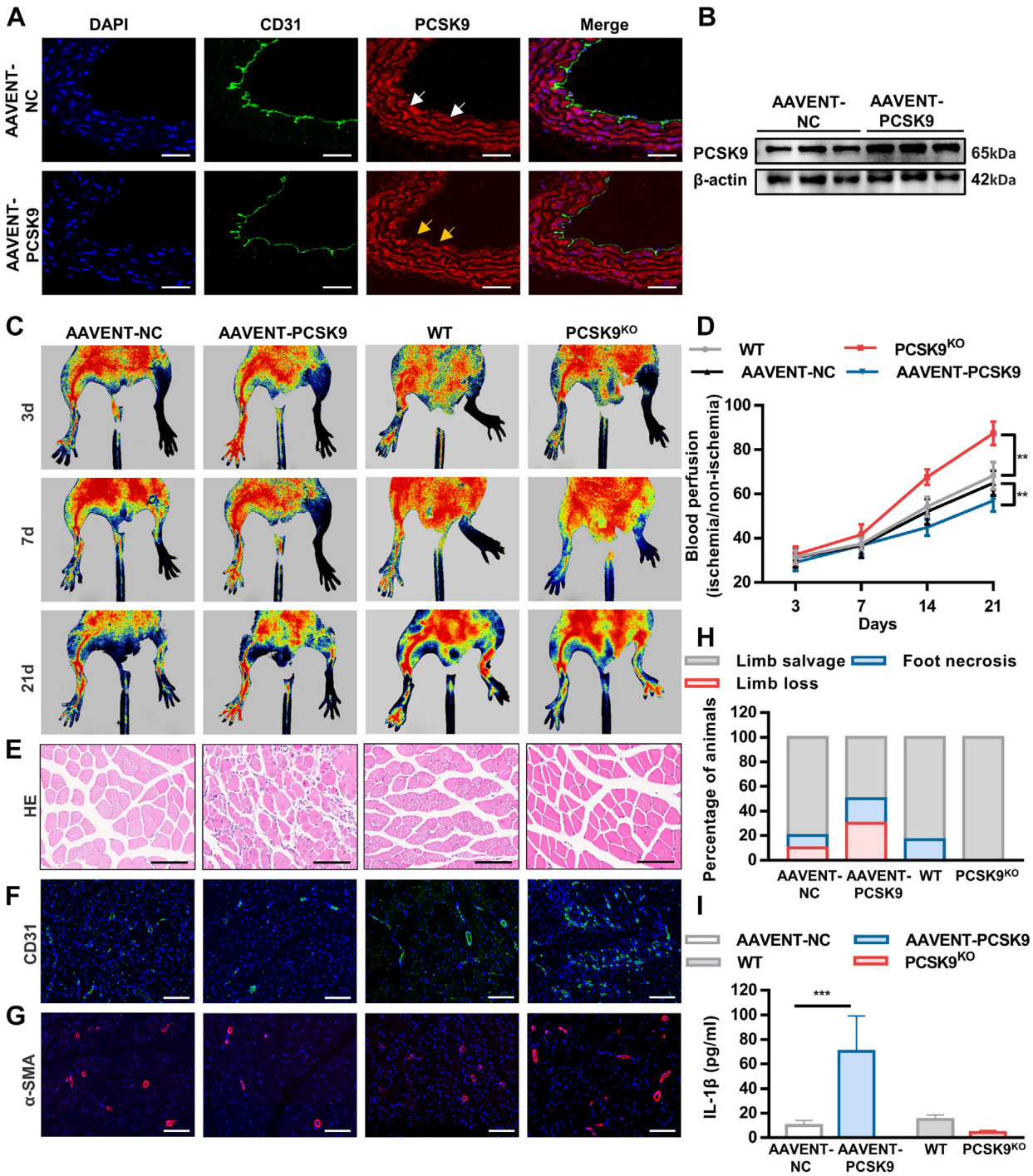

(A and B) Efficiency of adeno-associated virus (AAV) injection as verified by immunofluorescent staining (magnification ×20, scale bar = 20 μm) and Western blotting. **(C and D)** Representative images and quantification of blood perfusion in the ischemic hindlimb in the AAVENT-PCSK9 and PCSK9^{KO} groups. **(E)** Representative hematoxylin and eosin staining of muscle from the ischemic lower extremities of mice (magnification ×20, scale bar = 100 μm). **(F and G)** CD31 staining and α-SMA staining of ischemic lower limb muscle sections (scale bar = 100 μm). **(H)** Quantification analysis to detect ischemic lower limb status. **(I)** The concentration of IL-1β in mouse serum. Data are expressed as mean ± SD. For AAVENT-NC and AAVENT-PCSK9, n = 10 per group; for wild-type and PCSK9^{KO}, n = 6 per group. *$P < 0.05$, **$P < 0.01$, ***$P < 0.001$. In data **D and I,** differences were compared between wild-type and PCSK9^{KO} or between AAVENT-NC and AAVENT-PCSK9 in 21 days. Data **D and I** were analyzed using unpaired Student's *t*-test.

myocardial infarction. However, few studies have focused on the involvement of ECs in PCSK9-related pyroptosis.

Our results showed that PCSK9 was highly expressed in ECs under hypoxic conditions. We then recruited CLI patients and healthy subjects and tested the plasma level of PCSK9, which was higher in the CLL patients. PCSK9 expression was also higher in the distal hypoxic vascular endothelium than in the proximal normal vascular endothelium. Therefore, we investigated whether PCSK9 participates in hypoxia-induced pyroptosis in ECs to influence angiogenesis.

We found that suppressing the expression of PCKS9 alleviated hypoxia-induced pyroptosis. The result showed that PCSK9 participates in hypoxia-induced pyroptosis. However, it is not clear whether inhibition of PCSK9 improves lower limb ischemia by promoting angiogenesis.

We found that in vitro overexpression of PCSK9 inhibited the proliferation, migration, adhesion, and angiogenesis of vascular ECs. In mice with lower limb ischemia, PCSK9 overexpression ameliorated blood flow in the ischemic lower limbs. Knockout of PCSK9 expression significantly reduced the release of inflammatory factors after ligation and increased blood flow to ischemic lower limb. However, how PCSK9 mediates hypoxia-induced pyroptosis remains unknown.

Previous studies have shown that PCSK9 can mediate pyroptosis through the mitochondrial pathway, and mitochondrial protein translocation-related cell death has attracted a growing amount of attention in recent years.[32,33] Smac, a mitochondrial protein, is released into the cytoplasm in response to stimuli, including hypoxia, and then activates the caspase family, ultimately participating in cell death.[34] Therefore, we hypothesized that PCSK9 mediates hypoxia-induced pyroptosis through translocation of the mitochondrial protein Smac, thereby inhibiting angiogenesis. We found that PCSK9 knockdown reduced the expression of Smac and inhibited Smac release into the cytoplasm, while PCSK9 overexpression had the opposite effects. These results were then confirmed by immunofluorescence. Further studies showed that CsA inhibited PCSK9-mediated hypoxia-induced pyroptosis.

STUDY LIMITATIONS. First, further research is required to comprehend how PCSK9 mediates Smac mitochondria-cytoplasm translocation in HUVECs. Second, whether the application of PCSK9 inhibitor could contribute to recovery in CLI also merits further clinical study and validation.

CONCLUSIONS

Our study indicates that PCSK9 induces hypoxia-induced vascular EC pyroptosis via Smac mitochondrion-cytoplasm translocation. The present study provides novel insight into the potential of PCSK9 as a target for lower limb ischemia.

ACKNOWLEDGMENTS The authors thank the professors from Sun Yat-sen University for their technical assistance. Springer Nature provided language editing service. The visual abstract was created with BioRender.com.

FUNDING SUPPORT AND AUTHOR DISCLOSURES

This work was supported by the National Nature Science Foundation of China (82170427), Scientific and Technological Innovation Funding of Shenzhen (JCYJ20220530144601003), Medical Scientific Research Foundation of Guangdong (A2021045), Scientific and Technological Innovation Funding of Shenzhen (JCYJ20180306180229307), Sun Yat-sen University Clinical Medicine Research 5010 Cultivation Project (2018027), and Scientific Research Foundation of Futian District (FTWS2020009). The authors have reported that they have no relationships relevant to the contents of this paper to disclose.

ADDRESS FOR CORRESPONDENCE: Dr Jianwen Liang, Department of Cardiology, The Eighth Affiliated Hospital, Sun Yat-sen University, Shenzhen, Guangdong 518000, China. E-mail: liangjw39@mail.sysu.edu.cn. OR Dr Guifu Wu, Department of Cardiology, The Eighth Affiliated Hospital, Sun Yat-sen University, Shenzhen, Guangdong 518000, China. E-mail: wuguifu@mail.sysu.edu.cn.

PERSPECTIVES

COMPETENCY IN MEDICAL KNOWLEDGE: CLI is characterized by hypoxia-induced EC death and impaired angiogenesis. Our study demonstrates that PCSK9 aggravates hypoxia-induced pyroptosis by regulating Smac mitochondrion-cytoplasm translocation in vascular ECs.

TRANSLATIONAL OUTLOOK: Targeting PCSK9 in ECs holds promise for the treatment of CLI. Future studies evaluating the potential therapeutic effect of clinically available drugs targeting PCSK9 in patients with CLI will accelerate the development of novel therapeutic strategies against CLI.

REFERENCES

1. Pei X, Kim H, Lee M, et al. Local delivery of cardiac stem cells overexpressing HIF-1α promotes angiogenesis and muscular tissue repair in a hind limb ischemia model. *J Control Release*. 2020;322:610–621.

2. Caradu C, Couffinhal T, Chapouly C, et al. Restoring endothelial function by targeting desert hedgehog downstream of Klf2 improves critical limb ischemia in adults. *Circ Res*. 2018;123:1053–1065.

3. Lee FY, Sun CK, Sung PH, et al. Daily melatonin protects the endothelial lineage and functional integrity against the aging process, oxidative stress, and toxic environment and restores blood flow in critical limb ischemia area in mice. *J Pineal Res*. 2018;65:e12489.

4. Bedoui S, Herold MJ, Strasser A. Emerging connectivity of programmed cell death pathways and its physiological implications. *Nat Rev Mol Cell Biol*. 2020;21:678–695.

5. Liu X, Xia S, Zhang Z, Wu H, Lieberman J. Channelling inflammation: gasdermins in physiology and disease. *Nat Rev Drug Discov*. 2021;20:384–405.

6. Zhang K, Chai B, Ji H, et al. Bioglass promotes wound healing by inhibiting endothelial cell pyroptosis through regulation of the connexin 43/reactive oxygen species (ROS) signaling pathway. *Lab Invest*. 2022;102:90–101.

7. Salaun E, Mahjoub H, Dahou A, et al. Hemodynamic deterioration of surgically implanted bioprosthetic aortic valves. *J Am Coll Cardiol*. 2018;72:241–251.

8. Jang HD, Lee SE, Yang J, et al. Cyclase-associated protein 1 is a binding partner of proprotein convertase subtilisin/kexin type-9 and is required for the degradation of low-density lipoprotein receptors by proprotein convertase subtilisin/kexin type-9. *Eur Heart J*. 2020;41:239–252.

9. Qi Z, Hu L, Zhang J, et al. PCSK9 (proprotein convertase subtilisin/kexin 9) enhances platelet activation, thrombosis, and myocardial infarct expansion by binding to platelet CD36. *Circulation*. 2021;143:45–61.

10. Hedayat AF, Park KH, Kwon TG, et al. Peripheral vascular atherosclerosis in a novel PCSK9 gain-of-function mutant Ossabaw miniature pig model. *Transl Res*. 2018;192:30–45.

11. Liang J, Zhang X, Xia W, et al. Promotion of aerobic exercise induced angiogenesis is associated with decline in blood pressure in hypertension: result of EXCAVATION-CHN1. *Hypertension*. 2021;77:1141–1153.

12. Li H, Nguyen H, Meda Venkata SP, et al. Novel role of GPR35 (G-protein-coupled receptor 35) in the regulation of endothelial cell function and blood pressure. *Hypertension*. 2021;78:816–830.

13. Yu BB, Zhi H, Zhang XY, et al. Mitochondrial dysfunction-mediated decline in angiogenic capacity of endothelial progenitor cells is associated with capillary rarefaction in patients with hypertension via downregulation of CXCR4/JAK2/SIRT5 signaling. *EBioMedicine*. 2019;42:64–75.

14. He J, Liu X, Su C, et al. Inhibition of mitochondrial oxidative damage improves reendothelialization capacity of endothelial progenitor cells via SIRT3 (Sirtuin 3)-enhanced SOD2 (superoxide dismutase 2) deacetylation in hypertension. *Arterioscler Thromb Vasc Biol*. 2019;39:1682–1698.

15. Gerhard-Herman MD, Gornik HL, Barrett C, et al. 2016 AHA/ACC guideline on the management of patients with lower extremity peripheral artery disease: executive summary: a report of the American College of Cardiology/American Heart Association Task Force on Clinical Practice Guidelines. *J Am Coll Cardiol*. 2017;69(11):1465–1508.

16. Cheng SB, Nakashima A, Huber WJ, et al. Pyroptosis is a critical inflammatory pathway in the placenta from early onset preeclampsia and in human trophoblasts exposed to hypoxia and endoplasmic reticulum stressors. *Cell Death Dis*. 2019;10:927.

17. Sabatine MS. PCSK9 inhibitors: clinical evidence and implementation. *Nat Rev Cardiol*. 2019;16:155–165.

18. Schwartz GG, Steg PG, Szarek M, et al. Peripheral artery disease and venous thromboembolic events after acute coronary syndrome: role of lipoprotein(a) and modification by alirocumab: prespecified analysis of the ODYSSEY OUTCOMES Randomized Clinical Trial. *Circulation*. 2020;141:1608–1617.

19. Bernard NJ. Mitochondria control pyroptosis. *Nat Immunol*. 2021;22:1071.

20. Bauer TM, Murphy E. Role of mitochondrial calcium and the permeability transition pore in regulating cell death. *Circ Res*. 2020;126:280–293.

21. Saita S, Nolte H, Fiedler KU, et al. PARL mediates Smac proteolytic maturation in mitochondria to promote apoptosis. *Nat Cell Biol*. 2017;19:318–328.

22. Heilig R, Dilucca M, Boucher D, et al. Caspase-1 cleaves Bid to release mitochondrial SMAC and drive secondary necrosis in the absence of GSDMD. *Life Sci Alliance*. 2020;3(6):e202000735.

23. Karch J, Molkentin JD. Regulated necrotic cell death: the passive aggressive side of Bax and Bak. *Circ Res*. 2015;116:1800–1809.

24. Duan C, Kuang L, Hong C, et al. Mitochondrial Drp1 recognizes and induces excessive mPTP opening after hypoxia through BAX-PiC and LRRK2-HK2. *Cell Death Dis*. 2021;12:1050.

25. Zhou H, Wang J, Jiang J, et al. N-acetyl-serotonin offers neuroprotection through inhibiting mitochondrial death pathways and autophagic activation in experimental models of ischemic injury. *J Neurosci*. 2014;34:2967–2978.

26. Adams GN, Stavrou EX, Fang C, et al. Prolylcarboxypeptidase promotes angiogenesis and vascular repair. *Blood*. 2013;122:1522–1531.

27. Zhang J, Muri J, Fitzgerald G, et al. Endothelial lactate controls muscle regeneration from ischemia by inducing M2-like macrophage polarization. *Cell Metab*. 2020;31:1136–1153.e7.

28. Marushima A, Nieminen M, Kremenetskaia I, et al. Balanced single-vector co-delivery of VEGF/PDGF-BB improves functional collateralization in chronic cerebral ischemia. *J Cereb Blood Flow Metab*. 2020;40:404–419.

29. Annex BH, Cooke JP. New directions in therapeutic angiogenesis and arteriogenesis in peripheral arterial disease. *Circ Res*. 2021;128:1944–1957.

30. Kesavardhana S, Malireddi RKS, Kanneganti TD. Caspases in cell death, inflammation, and pyroptosis. *Annu Rev Immunol*. 2020;38:567–595.

31. Maxwell KN, Fisher EA, Breslow JL. Overexpression of PCSK9 accelerates the degradation of the LDLR in a post-endoplasmic reticulum compartment. *Proc Natl Acad Sci U S A*. 2005;102:2069–2074.

32. Wang X, Li X, Liu S, et al. PCSK9 regulates pyroptosis via mtDNA damage in chronic myocardial ischemia. *Basic Res Cardiol*. 2020;115:66.

33. Hamacher-Brady A, Choe SC, Krijnse-Locker J, Brady NR. Intramitochondrial recruitment of endolysosomes mediates Smac degradation and constitutes a novel intrinsic apoptosis antagonizing function of XIAP E3 ligase. *Cell Death Differ*. 2014;21:1862–1876.

34. Hui KK, Kanungo AK, Elia AJ, Henderson JT. Caspase-3 deficiency reveals a physiologic role for Smac/DIABLO in regulating programmed cell death. *Cell Death Differ*. 2011;18:1780–1790.

KEY WORDS critical limb ischemia, PCSK9, pyroptosis, Smac, vascular endothelial cell

APPENDIX For a supplemental table and figures, please see the online version of this paper.